EFFECT OF CAPROCK RELATIVE PERMEABILITY ON CO_2 FLOW THROUGH IT

Iman Rahimzadeh Kivi[1,2*], Victor Vilarrasa[1,2,3], Roman Makhnenko[4]

[1] Institute of Environmental Assessment and Water Research, Spanish National Research Council (IDAEA-CSIC), Barcelona, Spain

[2] Associated Unit: Hydrogeology Group (UPC-CSIC), Barcelona, Spain

[3] Mediterranean Institute for Advanced Studies (IMEDEA), Spanish National Research Council (CSIC), Esporles, Spain

[4] Department of Civil & Environmental Engineering, University of Illinois at Urbana-Champaign, Urbana, Illinois, USA.

* Corresponding author e-mail: iman.rahimzadeh@idaea.csic.es

Abstract

Geologic carbon storage is needed to meet the climate goal of limiting global warming to 1.5 ºC. Injecting in deep sedimentary formations brings CO_2 to a supercritical state, yet less dense than the resident brine making it buoyant. Therefore, the assessment of the sealing capacity of the caprock lying above the storage reservoir is of paramount importance for the widespread deployment of geologic carbon storage. We perform laboratory-scale supercritical CO_2 injection into a representative caprock sample and employ numerical simulations to provide an in-depth understanding of CO_2 leakage mechanisms. We explore the effect of relative permeability curves on the potential CO_2 leakage through the caprock. We show that capillary breakthrough is unlikely to take place across a non-fractured caprock with low intrinsic permeability and high entry pressure. Rather, CO_2 leakage is dominated by the intrinsically slow molecular diffusion, favoring safe storage of CO_2 over geological time scales.

Keywords: *Geologic carbon storage, Sealing capacity, Capillary breakthrough, Molecular diffusion, Shale*

1. Introduction

The growing emissions of anthropogenic CO_2 into the atmosphere have given rise to global warming and, thus, climate change with well-known harmful environmental effects. Being aware of the urgent threat of climate change to the planet, the majority of countries worldwide adopted the Paris Agreement, which aims at limiting global warming to well below 2 ºC compared to the pre-industrial level. To achieve this objective, the Intergovernmental Panel on Climate Change (IPCC) suggests different mitigation strategies [1]. All these mitigation pathways project increasing shares of renewables, energy efficiency, and Carbon Capture and Storage (CCS). By approaching the limits of efficiency and currently inevitable carbon emissions in some sectors, hundreds of gigatonnes of CO_2 should be stored over the course of the 21st century to reach zero emissions. The CCS technology is expected to be more pronounced in the second half of the century, during which huge net negative emissions have to happen.

CCS consists in capturing CO_2 from stationary sources and permanently storing it underground, mainly in deep saline aquifers. The targeted strata are preferably located deep enough (>800 m) to bring CO_2 to a supercritical state. At high temperatures (i.e., T>31.04 °C) and pressures (i.e., P>7.38 MPa), the supercritical CO_2 has a liquid-like density and gas-like viscosity, guaranteeing high storativity and injectivity [2][3]. However, CO_2 density never exceeds that of the resident brine at these conditions [4]. As a result, CO_2 is buoyant and floats across the injection reservoir. An appropriate injection site should include a low-permeability and high-entry pressure caprock, lying immediately above the storage reservoir, to prevent CO_2 migration out of the storage reservoir. Otherwise, CO_2 may approach shallow aquifers, hosting potable water, or even get back to the surface, putting the primary goal of long-term CO_2 storage in danger and imposing additional negative environmental impacts [5][6]. The assessment of the caprock sealing capacity is thus of crucial significance in screening appropriate storage sites and bringing public acceptance to carbon capture and storage at large scales.

As the non-wetting fluid, CO_2 penetrates into the caprock in free phase if the differential pressure between CO_2 and brine (i.e., the capillary pressure) overcomes the capillary entry pressure P_0 of the pore network. CO_2 is expected to percolate through the caprock if another capillary threshold, called breakthrough pressure P_{brth} is exceeded [7]. Nevertheless, desaturation of the pore network establishes a two-phase flow in which the effective permeability to each phase (the intrinsic permeability multiplied by the phase relative permeability) governs the advection rate. The literature provides very limited experimental measurements of CO_2-brine relative permeability in tight clay-rich caprock representatives [8]. The lack of data on relative permeability curves imposes high uncertainties on the caprock sealing capacity assessment. Besides, CO_2 dissolves by up to 4 mol% into the resident brine under reservoir conditions, initiating diffusive transport in the aqueous phase [9]. There is a consensus that the leakage becomes advection-dominated once the breakthrough pressure is surpassed [7][10]. The reliability of this statement has yet to be investigated on the lab-scale under well-monitored

conditions. In this study, we conduct supercritical CO_2 injection experiments on a representative caprock sample, namely Opalinus Clay. We parametrize a two-phase flow model and simulate the experiment numerically to deal with the abovementioned flow complexities and the associated uncertainties. Through replicating the experimental observations, we provide an improved understanding of the flow mechanisms controlling CO_2 leakage through the caprock. We also address the sensitivity of CO_2 flow behavior to the relative permeability curve.

2. Methodology

2.1 Materials and experimental methods

We choose shaly facies of Opalinus Clay as a representative caprock for this study. Samples are retrieved from the Mont Terri underground laboratory site in Switzerland. We employ preliminary characterization techniques to measure the capillary and flow properties of the material. Mercury intrusion porosimetry provides a porosity of 12.5% and dominant pore throat diameter value of 0.015 micron. The Mercury Intrusion Capillary Pressure (MICP) curves are converted to a supercritical CO_2 intrusion into an initially brine-saturated specimen by taking a CO_2-brine interfacial tension of 30 mN/m and a shale-CO_2-brine contact angle of 40° [11]. The CO_2 saturation curve suggests a capillary entry pressure of approximately 4 MPa. The intrinsic permeability of the shale is measured in a single-phase steady-state brine flow experiment and is determined to be $3 \cdot 10^{-21}$ m^2 [12]. The injected brine has a chemical composition similar to the formation fluid to prevent possible chemical effects and swelling of the tested material.

After the permeability measurement, supercritical CO_2 is injected into the shale according to the procedure described in Makhnenko et al. [13]. The 10 mm thick and 35 mm in diameter specimen is tested under the oedometric conditions (Figure 1). The specimen is capped between two 6-mm thick porous stones with a porosity of 32%, an intrinsic permeability of 10^{-12} m^2, and low entry pressure of 0.01 MPa, which are initially saturated with brine. The upstream CO_2 controller increases the pressure to a value (~22 MPa), higher than the estimated breakthrough threshold to promote advective CO_2 flow through the specimen. The upstream valve is then closed and the upstream pressure variation resulting from CO_2 flow is continuously recorded. Meanwhile, the downstream controller keeps the downstream brine pressure constant at 8 MPa and measures the outflow volume. The temperature of all experimental equipment is also kept constant at 40 ºC throughout the experiment.

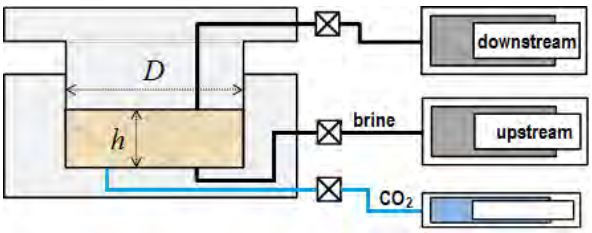

Figure 1: Schematic representation of the oedometric cell used to inject CO_2 into a cylindrical brine-saturated shale specimen of 10 mm thick and 35 mm in diameter

2.2 Numerical approach

CO_2 flow through the brine-saturated rock is a two-phase flow problem that requires solving the mass conservation for each phase (wetting and non-wetting) or each component (brine and CO_2). Adopting the latter approach, the mass balance equation writes as

$$\frac{\partial}{\partial t}(\omega_a^i \rho_a S_a \phi + \omega_c^i \rho_c S_c \phi) + \nabla.(\boldsymbol{i}_a^i + \boldsymbol{i}_c^i + \omega_a^i \rho_a \boldsymbol{q}_a + \omega_c^i \rho_c \boldsymbol{q}_c) = f^i, \quad (1)$$

where ϕ is porosity and t is time, ρ_ψ and S_ψ, in which the subscript ψ stands for either aqueous ($\psi = a$) or CO_2-rich phase ($\psi = c$), denote the phase density and saturation, respectively. ω_ψ^i represents the mass concentration of component i in phase ψ. The right-hand side f^i accounts for an external mass supply of component i. Mass transport includes phase advective flux of $\boldsymbol{q}_\psi$ and diffusive flux of individual components, $\boldsymbol{i}_\psi^i$.

The advective flow rate of each phase relates to pressure changes and gravity effect using Darcy´s law

$$\boldsymbol{q}_\psi = -\frac{\boldsymbol{k} k_{r\psi}}{\mu_\psi}(\nabla p_\psi + \rho_\psi g \nabla z), \quad (2)$$

where $\boldsymbol{k}$ is the intrinsic permeability, $k_{r\psi}$ is the relative permeability to the fluid phase ψ having a dynamic viscosity of μ_ψ, g is the gravity acceleration and z is the vertical position.

The molecular diffusion of components in each phase is expressed using Fick´s law

$$\boldsymbol{i}_\psi^i = -\tau \phi \rho_\psi S_\psi D_\psi^i \boldsymbol{I} \nabla \omega_\psi^i, \quad (3)$$

where τ stands for the pore structure tortuosity and D_ψ^i for the diffusion coefficient of component i in phase ψ, and $\boldsymbol{I}$ represents the identity tensor. The product of tortuosity and diffusion coefficient returns the effective diffusion coefficient D of each component through the rock.

It is worth mentioning that in an oedometric testing cell, the specimen is subjected to constant external stresses and hydromechanical coupling effects are minor due to relatively small pressure changes. Therefore, we here put our emphasis on the two-phase flow problem. A discussion on relevant hydromechanical coupling processes can be found in Rahimzadeh Kivi et al. [14].

Owing to the problem's symmetry, we take advantage of the low computational cost of an axisymmetric model. The model includes the shale specimen in the middle and

a set of stiff porous stone and loading platten on each upper and lower side (Figure 2). The fluid content of loading plattens reproduces the dead volumes of the testing setup.

The properties of the rock and porous stones are summarized in Table 1 and are used to calibrate a two-phase flow model. The aqueous phase saturation S_a relates to the capillary pressure p_{cap} through the Van Genuchten model [15]

$$S_{ea} = \frac{S_a - S_{ra}}{S_{max,a} - S_{ra}} = \left(1 + \left(\frac{p_{cap}}{p_0}\right)^{1/(1-m)}\right)^{-m}, \quad (4)$$

where S_{ra} and $S_{max,a}$ are residual and maximum brine saturations, respectively, S_{ea} is effective brine saturation, and m is the shape parameter of the retention curve. The parameters S_{ra}, $S_{max,a}$ and m are determined by fitting the experimentally obtained retention curves.

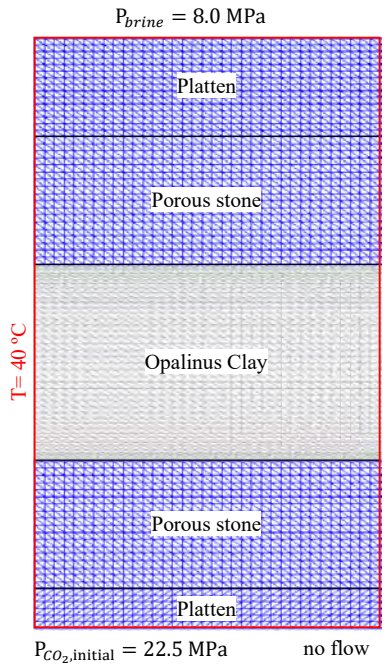

Figure 2: A sketch of the numerical model, including the mesh, for simulating the lab-scale CO_2 injection into the shale specimen

The relative permeability to each phase follows a power-law model with the corresponding effective saturation. Experimental evaluations of the relative permeability curves for clay-rich rock are rarely carried out due to their low permeability. An exponent of 6 is assumed to be appropriate for these geomaterials [8]. However, to deal with uncertainties associated with the relative permeability curves, we adapt a reference model with an exponent of 6 and perform a sensitivity analysis to this parameter. We use decreased exponent values of 5, 4 and 3. A lower one provides an increased preference for advection at a reference saturation degree (Figure 3). In this model, the relative permeability to CO_2 approaches unity at the residual brine saturation, although it can be much lower [8].

Table 1: Flow and retention properties of the Opalinus Clay and porous stones

Parameter	Opalinus Clay	Porous stones
Intrinsic permeability, k_0 (m^2)	$3 \cdot 10^{-21}$	10^{-12}
Rel. brine permeability, k_{ra}	S_{ea}^6	S_{ea}
Rel. CO_2 permeability, k_{rc}	$(1 - S_{ea})^6$	$1 - S_{ea}$
Residual brine saturation, S_{ra}	0.13	0
Max. brine saturation, $S_{max,a}$	1	1
Residual CO_2 saturation, S_{rc}	0	0
Gas entry pressure, P_0 (MPa)	3.83	0.01
van Genuchten constant, m	0.63	0.8
Initial porosity, ϕ_0	0.125	0.32
Diffusion coefficient, D (m^2/s)	$1.6 \cdot 10^{-9}$	$1.6 \cdot 10^{-9}$

CO_2 is injected at the bottom face and the upstream compartment is pressurized to 22.5 MPa. A no-flow boundary is then exerted and the system response to CO_2 flow is simulated. The temperature is maintained constant at 40 ºC throughout the simulation. We conduct the simulation using the finite element code CODE_BRIGHT [16], extended for CO_2 injection [17].

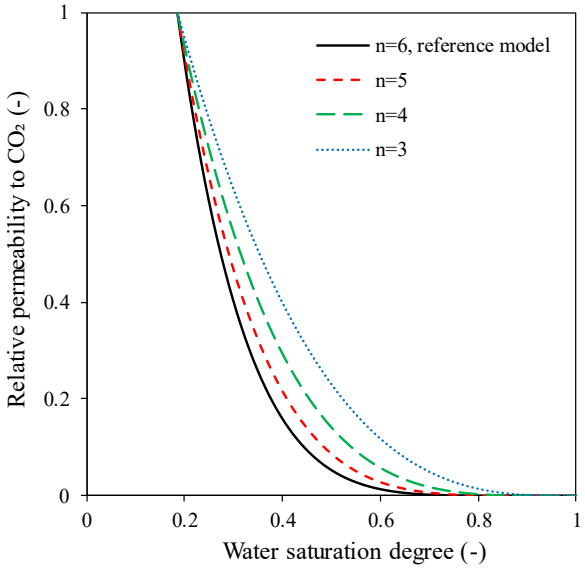

Figure 3: Relative permeability curves to CO_2 used in this study

3. Results and discussion

3.1 Reference case

Figure 4 illustrates the evolution of CO_2 pressure at the upstream side as well as the cumulative outflow volume at the downstream side. A logarithmic time scale is adopted to bring the short- and long-term responses together in one frame. The differential pressure between CO_2 and brine (~14.5 MPa) overcomes the capillary entry pressure of the specimen and CO_2 enters the pore network. Given the limited CO_2 supply at the upstream compartment, CO_2 pressure declines with time. CO_2 penetration into the specimen also gives rise to brine overpressure and an advective brine flow toward the downstream. Simulation results satisfactorily reproduce the observed pressure evolution in the short-term during

which experimental data are available. Nevertheless, simulations highly underestimate the outflow volume. This discrepancy can be attributed to the relative permeability curves we have used for the simulation and the presence of preferential flow paths through the tested shale specimen that are not considered by the model. These potential flow discontinuities may possess lower capillary entry pressure and higher permeability compared to the matrix, providing larger transported fluid volumes.

The long-term simulation results disclose a continuous CO_2 flow and pressure decrease until recovering a uniform pressure distribution throughout the specimen. To achieve a more detailed insight into the governing flow mechanisms, we draw the vertical profiles of brine saturation (Figure 5) and the individual components of CO_2 mass flux (Figure 6). CO_2 enters the pore network and commences desaturating the rock. As the CO_2 pressure propagates upward into the specimen, more interconnected pores experience drainage. However, the drainage path is not long-lasting and gives way to brine imbibition from the downstream because the upstream pressure continuously decreases. This drainage-to-imbibition transition happens after a short while (~10 hrs) at the upstream part of the specimen, while it takes more than 50 hours to occur downstream (Figure 5). From this moment on, the whole specimen imbibes brine from the downstream compartment until it becomes again fully saturated.

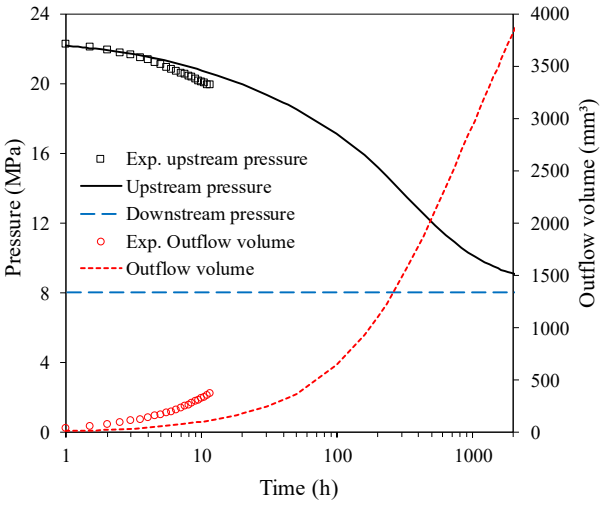

Figure 4: Results of supercritical CO_2 injection into the Opalinus Clay in terms of the upstream CO_2 pressure and downstream outflow volume. The calculated curves utilize a relative permeability model with an exponent of 6 (i.e., the reference model).

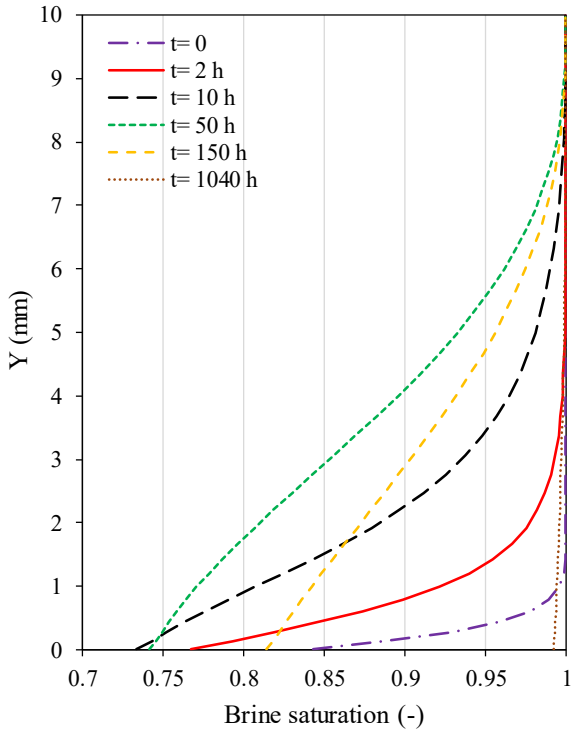

Figure 5: Distribution of brine saturation along the shale specimen and fluid compartments

Desaturation of the shale specimen promotes a two-phase flow of CO_2 and brine. According to Eq. (2), the advective CO_2 flux is directly linked to the corresponding relative permeability, which, in turn, is a function of saturation. In our reference model, an effective enhancement of the relative permeability can be expected if the brine saturation drops below 0.8 (see Figure 3). This extent of desaturation is observed only at the lowermost two millimeters of the 10-mm long specimen. For example, CO_2 saturation at a point located 2.5 mm away from the bottom face increases up to 0.17 but is insufficient to ever make CO_2 mobile. Therefore, the advective flux is quite concentrated around the bottom of the specimen and has negligible contribution to flow in the rest of the specimen (Figure 6). As a result, molecular diffusion thoroughly overwhelms the advective-driven behavior and stands merely as the dominating flow process. On the other hand, brine also advects across the specimen and conveys CO_2 in dissolution. Nevertheless, this mechanism has a negligible effect on the CO_2 mass transported and is thereby not included in Figure 6.

Interestingly, we infer from a sensitivity analysis on the specimen length (not shown here) that CO_2 injection into a longer specimen gives rise to an enhanced brine pressure buildup or equivalently decreased capillary pressure and, thus, specimen desaturation. This scale dependence can be more pronounced in the field where caprock thickness is in tens to hundreds of meters. Therefore, potential CO_2 leakage through shaly caprock favorably remains diffusion-dominated.

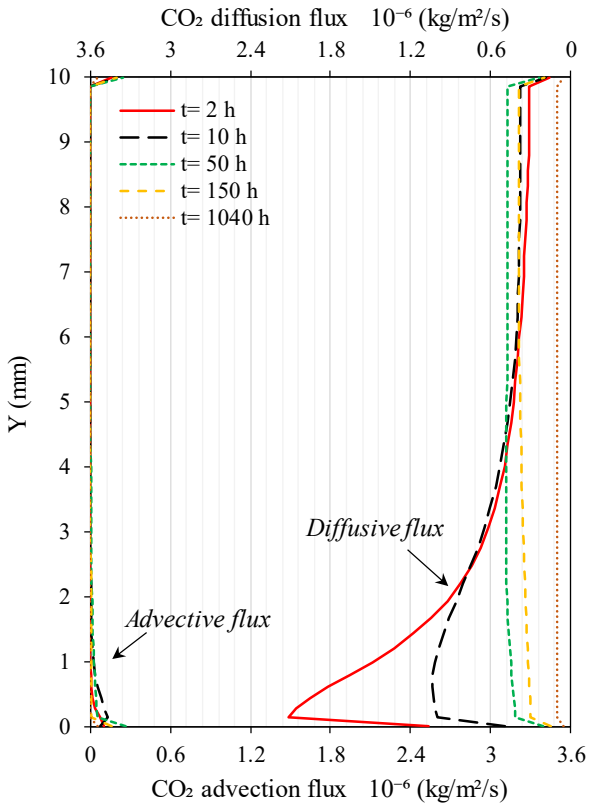

Figure 6: Vertical profiles of CO_2 flux components at several times: molecular diffusion and advection.

3.2 Sensitivity study on the relative permeability

The advancement of the advective CO_2 front depends on the relative permeability curve. The smaller the exponent n of the relative permeability model, the higher is the relative permeability and, thus, the further the advective front advances into the specimen. We here examine the sensitivity of the system behavior to relative permeabilities with lower exponents down to 3. Following our above reasoning, the worst scenario to the caprock sealing capacity is expected for the lowest exponent, i.e., n=3, which is presented in this study. Figure 7 displays a comparison between numerical simulations and experimental data. Provided a lower resistance to advection by the increased relative permeability, both the outflow volume and the pressure drop in the short term increase, compared to the reference case (see Figure 4). These changes provide an almost perfect fit to the recorded pressure data, though simulations are still far from a satisfactory match with the outflow volumes. However, the long-term simulation results are very similar in both cases. The upstream pressure and the outflow volume continue to evolve with time. To explore possible changes in flow mechanisms with the relative permeability curve and to reason the negligible difference between the two simulations, we plot vertical profiles of CO_2 mass flux terms in Figure 8. During early times (up to 30 hrs), the advective CO_2 flux along the specimen peaks at larger values than in the reference case. Moreover, the advective front propagates much further into the specimen (more than half of its length) compared to the reference case. CO_2 bubbles become mobile in the middle of the specimen. The advective flux assists in CO_2 mass transport, particularly during early times, whose effects have been reflected in Figure 7 as enhanced pressure drop and fluid discharge. Nevertheless, CO_2 flow at the downstream side remains purely diffusion-dominated. Simulations with intermediate relative permeability exponents (i.e., n=4 and n=5) consistently imply that decreasing the exponent n further restricts the advective flow to the lower part of the specimen.

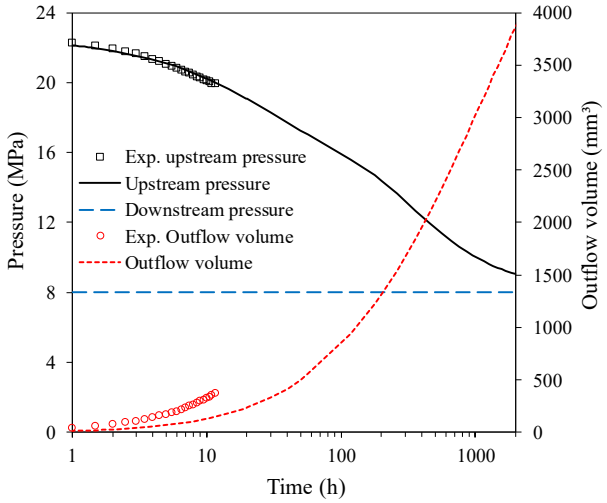

Figure 7: Results of supercritical CO_2 injection into the Opalinus Clay. The numerical simulation utilizes an enhanced relative permeability model with an exponent of 3.

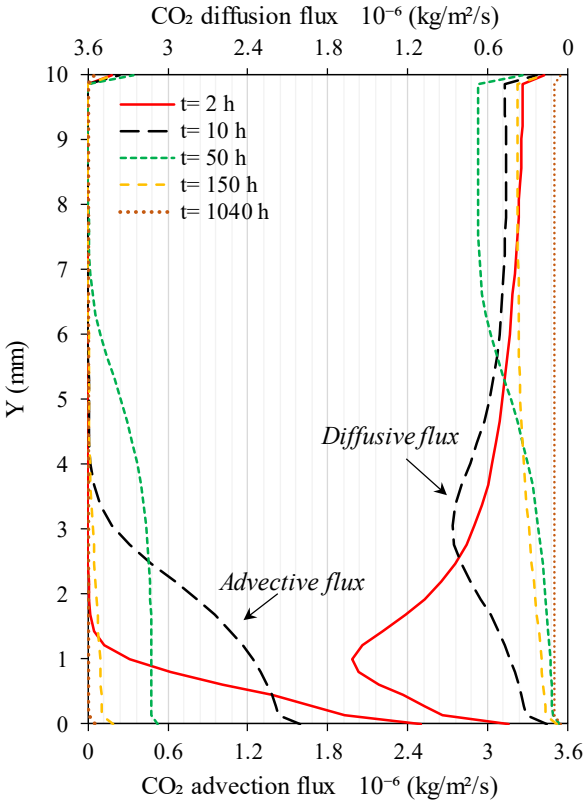

Figure 8: Vertical profiles of CO_2 flux components at several times obtained from numerical simulations with an exponent of 3 in the relative permeability model.

4. Summary and conclusions

Using numerical simulations of laboratory-scale supercritical CO_2 injection into a low-permeability Opalinus Clay (shale) we assess flow mechanisms governing potential CO_2 leakage through a non-fractured caprock. By overcoming the capillary entry pressure, CO_2 enters the rock and develops a two-phase flow. The advective CO_2 flow peaks at early times and the bottom face of the specimen experiences imbibition. The relative permeability to CO_2 locally increases and CO_2 advection remains confined to the lowermost portion of the rock with negligible contribution to flow. Even by changing the relative permeability curve, which leads to enhanced effective permeability to CO_2, the advective front does not bridge the specimen. Our analyses show that CO_2 transport through the representative caprock is dominated by molecular diffusion. Over the length and time span of interest in the field-scale CO_2 injection, it is unlikely that capillary breakthrough takes place and compromises the caprock sealing capacity. Yet, small fractions of CO_2 may diffuse across the caprock over geological time scales.

Acknowledgements

I.R.K. and V.V. acknowledge funding from the European Research Council (ERC) under the European Union's Horizon 2020 Research and Innovation Program through the Starting Grant GEoREST (www.georest.eu) (Grant agreement No. 801809). IDAEA-CSIC is a Centre of Excellence Severo Ochoa (Spanish Ministry of Science and Innovation, Project CEX2018-000794-S). R.M. is thankful for the support from US DOE through CarbonSAFE Macon County Project DE-FE0029381.

References

[1] IPCC, 2018: "Global Warming of 1.5°C. An IPCC Special Report on the impacts of global warming of 1.5°C above pre-industrial levels and related global greenhouse gas emission pathways, in the context of strengthening the global response to the threat of climate change, sustainable development, and efforts to eradicate poverty" [Masson-Delmotte, V., P. Zhai, H.-O. Pörtner, D. Roberts, J. Skea, P.R. Shukla, A. Pirani, W. Moufouma-Okia, C. Péan, R. Pidcock, S. Connors, J.B.R. Matthews, Y. Chen, X. Zhou, M.I. Gomis, E. Lonnoy, T. Maycock, M. Tignor, and T. Waterfield (eds.)].

[2] Bachu, S. (2003). Screening and ranking of sedimentary basins for sequestration of CO_2 in geological media in response to climate change. Environmental Geology, 44(3), 277-289.

[3] Celia, M. A. (2017). Geological storage of captured carbon dioxide as a large-scale carbon mitigation option. Water Resources Research, 53(5), 3527–3533.

[4] Vilarrasa, V., Bolster, D., Dentz, M., Olivella, S., Carrera, J., 2010. Effects of CO_2 compressibility on CO_2 storage in deep saline aquifers. Transp. Porous Media, 85, 619-639.

[5] Birkholzer, J. T., Zhou, Q., Tsang, C.-F. (2009). Large-scale impact of CO_2 storage in deep saline aquifers: a sensitivity study on pressure response in stratified systems. International Journal of Greenhouse Gas Control, 3, 181–194.

[6] Vilarrasa, V., Rutqvist, J., & Rinaldi, A. P. (2015). Thermal and capillary effects on the caprock mechanical stability at In Salah, Algeria. Greenhouse Gases: Science and Technology, 5(4), 449–461

[7] Hildenbrand, A., Schlomer, S., & Krooss, B. M. (2002). Gas breakthrough experiments on fine-grained sedimentary rocks. Geofluids 2(1), 3–23.

[8] Bennion, B., & Bachu, S. (2008). Drainage and imbibition relative permeability relationships for supercritical CO_2/brine and H_2S/brine systems in intergranular sandstone, carbonate, shale, and anhydrite rocks. SPE Reservoir Evaluation & Engineering, 11(3), 487-496.

[9] Gherardi, F., Xu, T., & Pruess, K. (2007). Numerical modeling of self-limiting and self-enhancing caprock alteration induced by CO_2 storage in a depleted gas reservoir. Chemical Geology, 244, 103–129.

[10] Espinoza, D. N., & Santamarina, J. C. (2017). CO_2 breakthrough-caprock sealing efficiency and integrity for carbon geological storage. International Journal of Greenhouse Gas Control, 66, 218–229.

[11] Espinoza, D. N., & Santamarina, J. C. (2010). Water-C-mineral systems: interfacial tension, contact angle and diffusion–Implications to CO_2 geological storage. Water Resources Research, 46, (W07537)

[12] Kim, K., & Makhnenko, R. (2020). Coupling between poromechanical behavior and fluid flow in tight rock. Transport in Porous Media, 135, 487-512.

[13] Makhnenko, R. Y., Vilarrasa, V., Mylnikov, D., & Laloui, L. (2017). Hydromechanical aspects of CO_2 breakthrough into Clay-rich caprock. Energy Procedia, 114, 3219–3228.

[14] Kivi, I. R., Vilarrasa, V., & Makhnenko, R. Y. (2020). Laboratory and numerical assessment of potential CO_2 leakage through the caprock. CouFrac2020, November 11–13, 2020, Seoul, Korea, in press.

[15] Van Genuchten, M. T. (1980). A closed-form equation for predicting the hydraulic conductivity of unsaturated soils. Soil Science Society of America Journal, 44(5), 892.

[16] Olivella, S., Carrera, J., Gens, A., & Alonso, E. E. (1994). Nonisothermal multiphase flow of brine and gas through saline media. Transport in Porous Media, 15(3), 271–293.

[17] Vilarrasa, V., Bolster, D., Olivella, S., & Carrera, J. (2010). Coupled hydromechanical modeling of CO_2 sequestration in deep saline aquifers. International Journal of Greenhouse Gas Control, 4(6), 910–919.